Michigan State University

National Superconducting Cyclotron Laboratory

MULTIFRAGMENT EMISSION IN $^{36}Ar + ^{197}Au$ and $^{129}Xe + ^{197}Au$ COLLISIONS: PERCOLATION MODEL

L. PHAIR, W. BAUER, D.R. BOWMAN, N. CARLIN, R.T. de SOUZA, C.K. GELBKE, W.G. GONG, Y.D. KIM, M.A. LISA, W.G. LYNCH, G.F. PEASLEE, M.B. TSANG, C. WILLIAMS, F. ZHU, N. COLONNA, K. HANOLD, M.A. McMAHAN, G.J. WOZNIAK, and L.G. MORETTO

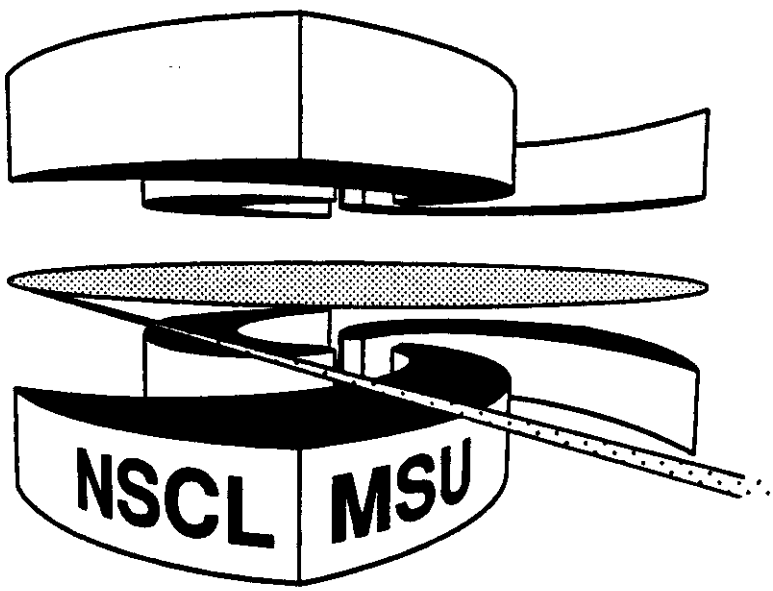

MSUCL-819

JANUARY 1992

MSUCL-819
January, 1992

Multifragment emission in $^{36}Ar+^{197}Au$ and $^{129}Xe+^{197}Au$ collisions: percolation model.

L. Phair, W. Bauer, D.R. Bowman, N. Carlin,[†] R.T. de Souza,[††]
C.K. Gelbke, W.G. Gong? [††] Y.D. Kim,[††] M.A. Lisa, W.G. Lynch,
G.F. Peaslee, M.B. Tsang, C. Williams, and F. Zhu

National Superconducting Cyclotron Laboratory
and Department of Physics and Astronomy
Michigan State University, East Lansing, *MI 48824*

N. Colonna, K. Hanold, M.A. McMahan,
G.J. Wozniak, and L.G. Moretto

Nuclear Science Division and Accelerator and Fusion Research Division
Lawrence Berkeley Laboratory, Berkeley, CA. 94720

Abstract

Relative abundances of intermediate mass fragments and light particles measured for $^{36}Ar+^{197}Au$ collisions at E/A=50, 80 and 110 MeV lie within the range of percolation model predictions, but for $^{129}Xe+^{197}Au$ collisions at E/A=50 MeV, the percolation model predicts too few fragments.

---

t Present address: Instituto de Física, Universidade de São Paulo, C. Postal 20516, CEP 01498, São Paulo, Brazil

†† Present address: IUCF and Department of Chemistry, Indiana University, Bloomington, IN 47405

t †† Present address: Nuclear Science Division, Lawrence Berkeley Laboratory, Berkeley, CA 94720

Multifragment disintegrations of highly excited nuclear systems might carry information about the equation of state and the liquid gas phase transition of low density nuclear matter [1-6 and references given therein]. In rather general terms [1,3], the fluctuations at the critical point of the nuclear matter phase diagram are expected to lead to mass distributions which follow a power law, $\sigma(A) \propto A^{-\tau}$, with a critical exponent of the order of $\tau \approx 2.2\text{-}2.3$. A number of theoretical investigations of phase transitions in finite nuclear systems have been based on percolation models [7-14]. Percolation models are attractive, since they exhibit a well-defined phase transition for infinite systems and since they allow straightforward generalizations to finite systems and the incorporation of important geometrical ingredients [13] for multifragmenting systems. Percolation models have also been useful for the development of techniques to extract critical exponents from exclusive fragmentation data [11,12]. Most percolation models are, however, governed by a single bond-breaking or site-vacancy parameter and cannot be expected to reproduce the two-dimensional phase diagram of nuclear matter in the temperature *vs.* density plane. Despite this limitation, percolation models have been rather successful [7-9] in describing the observed [3] power-law behavior of measured fragment mass distributions and in developing techniques to extract critical exponents. In this letter, we provide a test of the bond-percolation model of refs. [7-9] and compare its predictions to fragment yields measured with a low-threshold 4π detector for the reactions ^{129}Xe+^{197}Au at E/A=50 MeV and ^{36}Ar+^{197}Au at E/A=50, 80, 110 MeV.

The experiments were performed with beams from the K1200 cyclotron of the NSCL at Michigan State University. Reaction products were detected with the MSU Miniball phoswich detector array [15]. Each phoswich detector consisted of a 40 μm thick plastic scintillator foil backed by a 2 cm thick CsI(Tl)

crystal. (For detectors in Ring 1, the scintillator foil was 50 μm thick.) For the ^{129}Xe+^{197}Au reaction, the most forward angles were covered by a 16-element hodoscope, each element of which consisted of two position-sensitive solid-state detectors (300 μm and 5 mm thick) and a 7.6 cm thick plastic scintillator [16]. Fragments detected in the Miniball were identified by element for Z≈1-20; representative detection thresholds were 2, 3, and 4 MeV/nucleon for Z=3, 10, and 18 fragments, respectively. Fragments detected in the forward array were identified by element for Z=1-54; representative detection thresholds were 6, 13, 21, and 27 MeV/nucleon for Z=2, 8, 20, and 54 fragments, respectively. Additional technical details and details of the detector geometries can be found in refs. [15-18].

For a given event, we define the charged particle multiplicity N_C as the number of detectors in which at least one charged particle is recorded, including low energy fragments stopped in the plastic scintillator foils. Previous analyses of the ^{36}Ar+^{197}Au [17] and ^{129}Xe+^{197}Au [18] reactions employed slightly different definitions of intermediate mass fragments (IMF, Z=3-20). Consistent with the definition adopted in ref. [18], IMF multiplicities presented in this paper do not include unidentified low energy fragments which were stopped in the plastic scintillator foils. As a result, the IMF multiplicities for the ^{36}Ar+^{197}Au reaction are slightly lower than those reported in ref. [17]. Uncertainties resulting from these different conventions for determining observed IMF multiplicities do not affect the conclusion of this paper.

Calculations were performed with the bond percolation model of ref. [7-9]. In this model, the nucleus is considered to be a cubic lattice, the sites of which are randomly occupied by protons and neutrons. Initially, all nucleons are connected in one cluster. The bonds between the sites are randomly broken with a

probability p. Each nucleon is assigned a random momentum consistent with the momentum distribution of a Fermi-gas of temperature T estimated [9] from the bond-breaking probability as $T=11.7\sqrt{p}$ MeV. Emitted fragments are defined in terms of connected clusters. Initial fragment energies are calculated from the total momenta of the clusters. Final kinetic energies are calculated by incorporating the final state Coulomb repulsion between the fragments. For this purpose a given fragment partition is translated into a spatial distribution of clusters characterized by an average freeze-out density $\rho=0.2\rho_0$, where $\rho_0=0.17$ fm^{-3} is the density of normal nuclear matter. (Different choices of the freeze-out density lead to slightly different shapes of the low energy portion of the energy spectrum due to changes in the Coulomb repulsion between the fragments. Such changes are of minor importance for the present investigation.) The final momenta of the emitted fragments are boosted by the velocity of the center-of-mass of projectile and target. In order to allow meaningful comparisons with our data, we have filtered the theoretical distributions with the response of the experimental apparatus.

Elemental multiplicity distributions measured for the reactions ^{36}Ar+^{197}Au and ^{129}Xe+^{197}Au are shown (as points) in the top and bottom panels of Fig. 1. These distributions were obtained by integrating all identified fragments over all detectors. In order to select central collisions, these Z-distributions were gated by the total charged particle multiplicity cuts indicated in the figure. These cuts were chosen to represent the range of impact parameters of $b \leq 0.3 b_{max}$ when one adopts a strictly geometric interpretation of the measured charged particle multiplicity [19]:

$$[b(N_C)/b_{max}]^2 = [\sum_{n_C=N_C}^{\infty} \sigma(n_C)] / [\sum_{n_C=2}^{\infty} \sigma(n_C)] \quad . \qquad (1)$$

Here, b_{max} is the reaction cross section for collisions in which at least two charged particles are detected and $\sigma(n_C)$ is the cross section for detecting n_C charged particles. The elemental distributions observed for the various reactions exhibit rather similar shapes. For the $^{36}Ar+^{197}Au$ system (top panel), the elemental multiplicity distributions become slightly steeper with increasing bombarding energy. The multiplicities for heavier IMFs are significantly larger for the $^{129}Xe+^{197}Au$ system (bottom panel) than for the $^{36}Ar+^{197}Au$ system (top panel). Part of this difference in the observed yields of heavier fragments may be due to an increased detection efficiency in $^{129}Xe+^{197}Au$ reactions resulting from the larger center-of-mass velocity.

The curves in Fig. 1 depict elemental multiplicities predicted by the bond percolation model of refs. [7-9] and filtered by the detection efficiency of the experimental apparatus. Calculations are shown for representative bond-breaking probabilities above and below the critical bond breaking parameter of p=0.7. (In the percolation model, the critical point marks a second order phase transition; for p>0.7, the percolation cluster disappears and the system breaks up completely.) Calculations performed for bond-breaking probabilities much larger or smaller than the critical value predict Z-distributions which are too steep. For the $^{36}Ar+^{197}Au$ reactions, the overall magnitudes and shapes of the experimental Z-distributions are in reasonable agreement with predictions of the percolation model when the bond breaking parameter is taken close to the critical value. However, for the $^{129}Xe+^{197}Au$ reaction, the percolation model underpredicts the yield of heavier fragments (Z≈6-20) for any choice of the bond breaking parameter.

Representative angular distributions of emitted particles are shown in Fig. 2. The top and bottom panels show results for the $^{36}Ar+^{197}Au$ reaction at

E/A=110 MeV and for the ^{129}Xe+^{197}Au reaction at E/A=50 MeV, respectively. The angular distributions are shown for three different ranges of element numbers, Z=1-2 (circles), Z=3-5 (squares), and Z=6-12 (diamonds). For both systems, the angular distributions become more forward peaked with increasing fragment charge. Angular distributions for the ^{129}Xe+^{197}Au system are more forward peaked than those for the ^{36}Ar+^{197}Au system. These effects are largely due to kinematics. Differences between the angular distributions of the two reactions arise primarily from the larger velocity of the emitting source of the Xe-Au system.

The curves in Fig. 2 show results of percolation calculations. To facilitate a better comparison of shapes between observed and predicted angular distributions, the calculated angular distributions were normalized to the experimental yields at θ=45°. To display the effects of the detector response, filtered and unfiltered calculations are shown by solid and dashed curves, respectively. In view of the fact that the percolation model does not include dynamical preequilibrium effects, the shapes of the experimental angular distributions are reasonably well reproduced by the calculations. Discrepancies between theoretical and experimental angular distributions due to preequilibrium emission are most pronounced for lighter fragments. For such fragments the measured angular distributions are slightly more forward peaked in the laboratory than the calculated angular distributions. Nevertheless, the angular distributions are sufficiently realistic to allow the assessment of instrumental distortions for the energy- and angle-integrated particle distributions presented in Figs. 1 and 3.

In order to display more clearly the fraction of IMFs among the emitted charged particles, Fig. 3 presents the average IMF multiplicity, $\langle N_{IMF} \rangle$, as a

function of charged particle multiplicity, N_C [17,18]. For a given charged particle multiplicity, more intermediate mass fragments are observed for the ^{129}Xe+^{197}Au reaction that for the ^{36}Ar+^{197}Au reactions. At large charged particle multiplicities ($N_C \gtrsim 30$), IMF admixtures of $\langle N_{IMF}\rangle/N_C \approx 0.18$ and 0.1 are observed for the systems ^{129}Xe+^{197}Au and ^{36}Ar+^{197}Au, respectively.

If the elemental distributions strictly followed a power law distribution, $\sigma(Z)=\sigma_0 Z^{-\tau}$, the IMF-admixture would be determined by the exponent τ:

$$N_{IMF}/N_C = [\sum_{Z=3}^{20} \sigma_0 Z^{-\tau}] / [\sum_{Z=1}^{Z_{max}} \sigma_0 Z^{-\tau}] \quad . \qquad (2)$$

For power law distributions, the (raw detected) ratios of $\langle N_{IMF}\rangle/N_C \approx 0.18$ and 0.10 correspond to exponents of $\tau \approx 2.15$ and 2.6. If one uses the shapes of the energy and angular distributions predicted by the percolation model to correct for the detector efficiency, one obtains efficiency corrected values of $\langle N_{IMF}\rangle/N_C \approx 0.19$ and 0.116, corresponding to $\tau \approx 2.12$ and 2.5. These values are slightly below and above the value, $\tau_{crit} \approx 2.2$, at the critical point.

According to Fig. 1, the percolation model underpredicts the yield of IMFs with $Z \gtrsim 5$ for the ^{129}Xe+^{197}Au reaction. This failure is displayed more clearly in Fig. 3 where we have evaluated the range of admixtures of IMFs among the emitted charged particles predicted by the percolation model for composite systems formed in ^{36}Ar+^{197}Au and ^{129}Xe+^{197}Au collisions. The shaded area represents the range of IMF admixtures calculated for bond-breaking parameters p=0.6-0.8. This range of bond-breaking parameters includes Z-distributions which are in rough agreement with our data (see Fig. 1). Larger

or smaller values of the bond-breaking parameter predict too steep charge distributions and, hence, lower IMF admixtures. For the lighter $^{36}Ar+^{197}Au$ system, the observed ratio $\langle N_{IMF} \rangle / N_C$ lies within the range of the percolation model predictions. However, for the heavier $^{129}Xe+^{197}Au$ system, maximum IMF admixtures compatible with the percolation model are smaller than the experimental values by nearly a factor of two.

High resolution coincidence experiments indicate that a significant portion of primary fragments can be expected to be produced in highly excited, particle unbound states which decay by light particle emission [20]. Such sequential decay processes will result in secondary fragment yields which are smaller and secondary light particle yields which are larger than the corresponding primary yields. The portion of primary fragments may therefore be even larger than the portion of particle-stable secondary fragments. This aggravates the failure of the percolation model to predict the large proportion of intermediate mass fragments among the particles emitted in the $^{129}Xe+^{197}Au$ reaction.

The inability of the bond-percolation model to reproduce the large intermediate mass fragment multiplicities observed for the $^{129}Xe+^{197}Au$ system is unexpected and represents, to our knowledge, the first significant failure of the percolation model. This model is only one representation of a large number of phase transition models, which all belong to the same universality class and should therefore show similar deficiencies. At present it is not clear whether one can rule out all such models or whether one may be forced to consider dynamical enhancements of fragment yields due to collective expansion or rotation.

This work is based upon work supported by the National Science Foundation under Grant numbers PHY-86-11210, PHY-89-13815, PHY-9017077 and the U.S. Department of Energy under Contract No. DE-AC03-76SF00098. W.G. Lynch acknowledges the receipt a of U.S. Presidential Young Investigator Award and N. Carlin acknowledges partial support by the FAPESP, Brazil.

References

1. P.J. Siemens, Nature **305** (1983) 410.
2. G. Bertsch and P.J. Siemens, Phys. Lett. **126B** (1983) 9.
3. A.S. Hirsch, A. Bujak, J.E. Finn, L.J. Gutay, R.W. Minich, N.T. Porile, R.P. Scharenberg, B.C. Stringfellow, and F. Turkot, Phys. Rev. **C29**, 508 (1984).
4. L.P. Cernai and J. Kapusta, Phys. Reports **131** (1986) 223.
5. W.G. Lynch, Ann. Rev. Nucl. Sci. **37** (1987) 493.
6. D.H.E. Gross, Rep. Prog. Phys. **53** (1990) 605.
7. W. Bauer, D.R. Dean, U. Mosel, and U. Post, Phys. Lett. **150B** (1985) 53.
8. W. Bauer, U. Post, D.R. Dean, and U. Mosel, Nucl. Phys. **A452** (1986) 699.
9. W. Bauer, Phys. Rev. **C38** (1988) 1927.
10. X. Campi, J. Phys. **A19** (1986) L917.
11. X. Campi, Phys. Lett. **208B** (1988) 351.
12. H. Ngô, C. Ngô, F.Z. Ighezou, J. Debois, S. Leray, and Y.-M. Zheng, Z. Phys. **A337** (1990) 81.
13. T.S. Biro, J. Knoll, and J. Richert, Nucl. Phys. **A459** (1986) 692.
14. H.R. Jaqaman, G. Papp, and D.H.E. Gross, Nucl. Phys. **A514** (1990) 327.
15. R.T. de Souza, N. Carlin, Y.D. Kim, J. Ottarson, L. Phair, D.R. Bowman, C.K. Gelbke, W.G. Gong, W.G. Lynch, R.A. Pelak, T. Peterson, G. Poggi, M.B. Tsang, and H.M. Xu, Nucl. Instr. and Meth. **A295** (1990) 109.
16. W.L. Kehoe et al., Lawrence Berkeley Laboratory preprint # LBL-31005.
17. R.T. de Souza, L. Phair, D.R. Bowman, N. Carlin, C.K. Gelbke, W.G. Gong, Y.D. Kim, M.A. Lisa, W.G. Lynch, G.F. Peaslee, M.B. Tsang, H.M. Xu, F. Zhu, and W.A. Friedman, Phys. Lett. **B268** (1991) 6.
18. D.R. Bowman, G.F. Peaslee, R.T. de Souza, N. Carlin, C.K. Gelbke, W.G. Gong, Y.D. Kim, M.A. Lisa, W.G. Lynch, L. Phair, M.B. Tsang, C. Williams, N. Colonna, K. Hanold, M.A. McMahan, G.J. Wozniak, L.G. Moretto, and W.A. Friedman, Phys. Rev. Lett. **67** (1991) 1527.

19. C. Cavata, M. Demoulins, J. Gosset, M.C. Lemaire, D. L'Hôte, J. Poitou, and O. Valette, Phys. Rev. **C42** (1990) 1760.

20. T.K. Nayak, T. Murakami, W.G. Lynch, K. Swartz, D.J. Fields, C.K. Gelbke, Y.D. Kim, J. Pochodzalla, M.B. Tsang, F. Zhu, and K. Kwiatkowski, Phys. Rev. Lett. **62** (1989) 1021, and refs. therein

Figure Captions

Fig. 1: Elemental multiplicity distributions detected in $^{36}Ar+^{197}Au$ collisions at E/A=50, 80, 110 MeV (top panel) and in $^{129}Xe+^{197}Au$ collisions at E/A=50 MeV (bottom panel). The curves represent calculations with the bond percolation model of refs. [7-9] for the indicated bond-breaking probabilities p. The calculations are filtered by the response of the experimental apparatus.

Fig. 2: Angular multiplicity distributions of light particles (Z=1,2: circles), and intermediate mass fragments of Z=3-5 (squares) and Z=6-12 (diamonds) detected in $^{36}Ar+^{197}Au$ collisions at E/A=50, 80, 110 MeV (top panel) and in $^{129}Xe+^{197}Au$ collisions at E/A=50 MeV (bottom panel). The curves represent calculations with the bond percolation model of refs. [7-9] for a bond-breaking probability of p=0.7. The calculations have been normalized to the data at θ=45°. Dashed and solid curves show raw calculations and calculations filtered by the response of the experimental apparatus.

Fig. 3: Relation between average IMF and charged particle multiplicities detected in $^{36}Ar+^{197}Au$ collisions at E/A=50, 80, 110 MeV (open diamonds, solid diamonds, squares respectively) and in $^{129}Xe+^{197}Au$ collisions at E/A=50 MeV (solid circles). The hatched area depicts the range of values covered by the bond-percolation model with bond breaking parameters p=0.6-0.8; the model predictions were filtered by the response of the experimental apparatus. For bond-breaking parameters outside this range, the predictions lie below N_{IMF}-values indicated by the cross-hatched area.

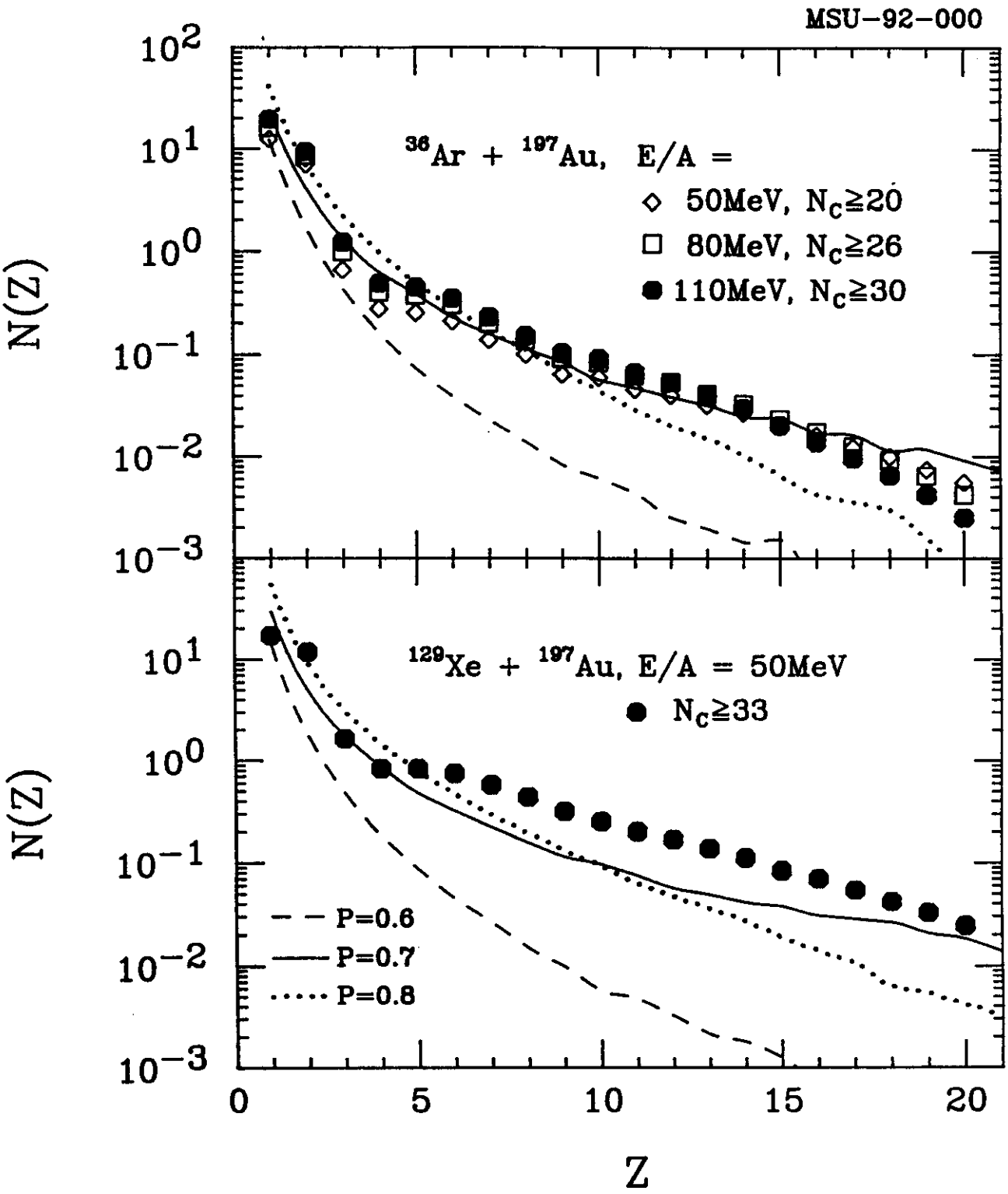
MSU-92-000
^{36}Ar + ^{197}Au, E/A =
50MeV, $N_c \geq 20$
80MeV, $N_c \geq 26$
110MeV, $N_c \geq 30$
^{129}Xe + ^{197}Au, E/A = 50MeV
$N_c \geq 33$
P=0.6
P=0.7
P=0.8
N(Z)
N(Z)
Z
10^2
10^1
10^0
10^{-1}
10^{-2}
10^{-3}
0
5
10
15
20

Fig. 1

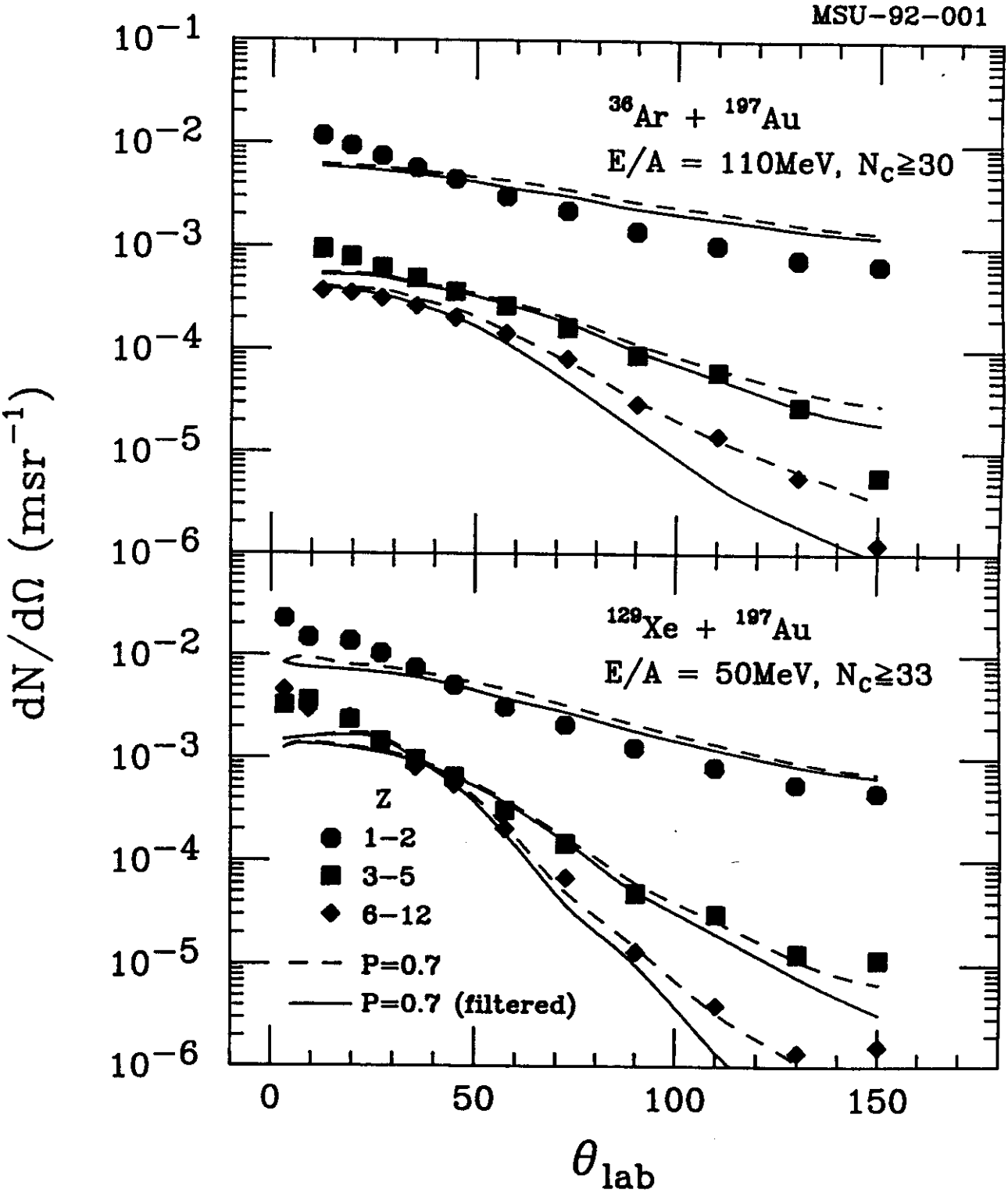
MSU-92-001
$^{36}Ar + ^{197}Au$
E/A = 110MeV, $N_c \geq 30$
$^{129}Xe + ^{197}Au$
E/A = 50MeV, $N_c \geq 33$
Z
1–2
3–5
6–12
P=0.7
P=0.7 (filtered)
10^{-1}
10^{-2}
10^{-3}
10^{-4}
10^{-5}
10^{-6}
0
50
100
150
θ_{lab}
$dN/d\Omega$ (msr^{-1})

Fig. 2

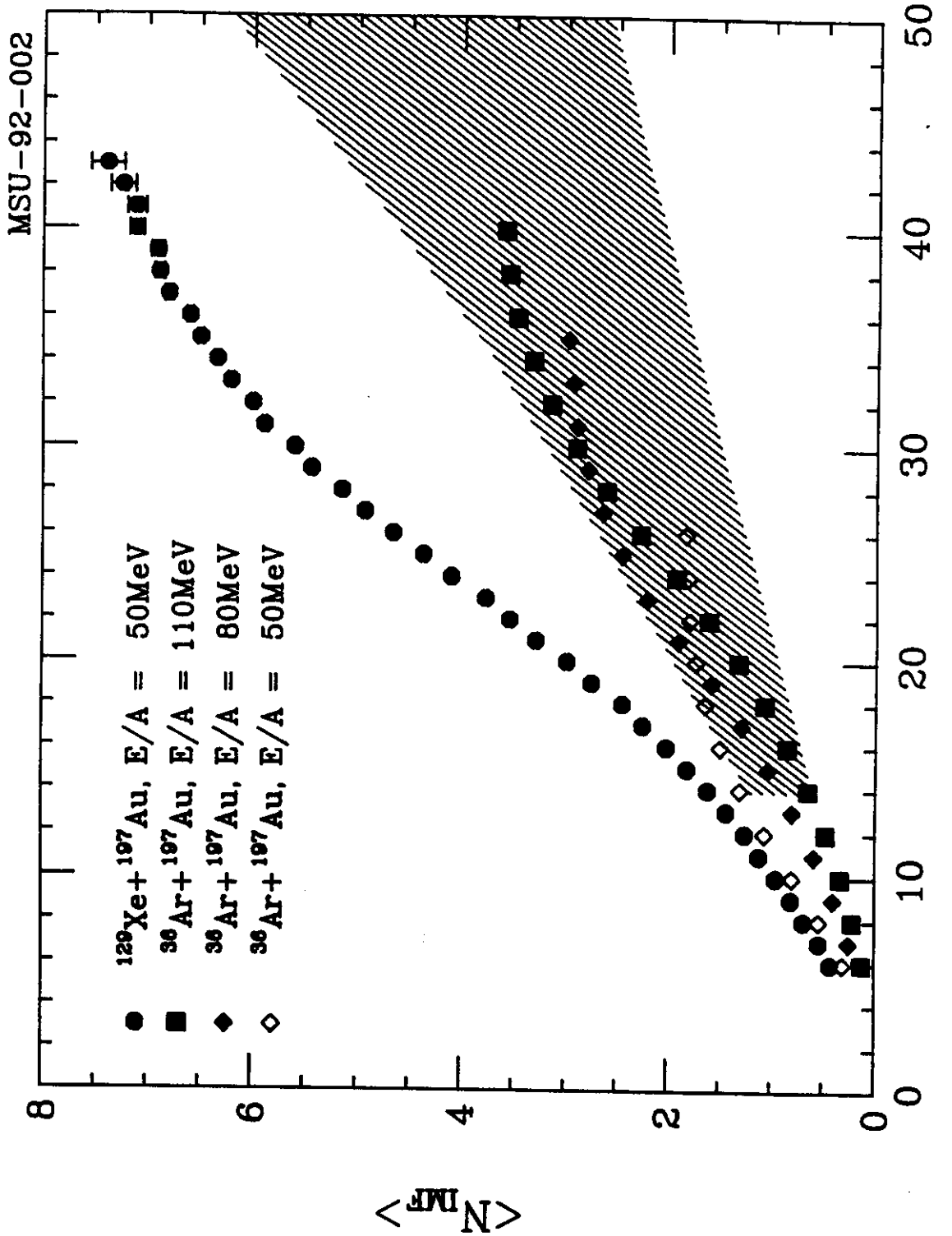
MSU-92-002
$^{129}Xe+^{197}Au$, E/A = 50MeV
$^{36}Ar+^{197}Au$, E/A = 110MeV
$^{36}Ar+^{197}Au$, E/A = 80MeV
$^{36}Ar+^{197}Au$, E/A = 50MeV
$\langle N_{IMF} \rangle$
N_C
0
2
4
6
8
0
10
20
30
40
50

Fig. 3